Supporting information

1-D polymeric and 2-D layered zinc monoalkyl phosphates bearing long alkyl chains: Synthesis, structural transformations and thermal behaviour

Harsha Arya and Ramaswamy Murugavel*

Department of Chemistry, Indian Institute of Technology Bombay, Powai, Mumbai-400076, India

E-mail: rmv@chem.iitb.ac.in

Fig. S1 FT-IR spectra of **1**, **2a,** and **2b** as KBr pellets

Fig. S2 FT-IR spectra of **3** and **4** as KBr pellets

Fig. S3 ^{31}P CP-MAS NMR spectra of **3** and **4** (303 MHz)

Fig. S4 Molecular structure of $[^{n}OctOPO_3Zn(DMF)]_n$ (**1**) (a) S4R ring in the polymeric structure (b) Edge sharing S4R rings

Fig.S5 Molecular structure of $[^{n}HexOPO_3Zn(DMF)]_n$ (**3**) (a) S4R ring in the polymeric structure (b) Edge sharing S4R rings

Fig. S6 Experimental and simulated Powder XRD pattern of **1**

Fig. S7 Experimental and simulated powder XRD pattern of **3**; pure experimental PXRD for **3** could not be obtained due to rapid solvent exchange

Fig. S8 SEM image of (a) **2a** and (b) **3** showing layered morphology

Fig. S9 Powder XRD patterns showing structure evolution of **4** from a mixture of **3** and **4**

Fig S10. PXRD patterns of **2a** before and after two hours of sonication in DMF at 50 ℃, followed by exposure to water

Fig S11. PXRD patterns of **4** before and after two hours of sonication in DMF at 50 ℃.

Fig S12. PXRD patterns of **2b** before and after heating at 50 ℃ under vacuum for 20 hours, showing its conversion back to **2a**

Fig S13. TGA curves of **2b** before and after heating at 50 ℃ under vacuum for 20 hours, indicating that **2a** and **2b** have similar chemical composition

Fig. S14. Variable temperature PXRD of **2b** showing the formation of an amorphous phase at 300 ℃ and a crystalline phase at 800 ℃ (* corresponds to the peaks due to platinum sample holder)

Fig. S15. Variable temperature PXRD plots of **2b** during (a) heating and (b) cooling, showing an increase in interlayer distance with increase in temperature

Fig. S16. Variable temperature PXRD plots of **4** during (a) heating, and (b) cooling, showing an increase in interlayer distance with increase in temperature

Fig. S17 TGA-DTA traces of (a) **1** and (b) **3** recorded under a flow of N_2 at a heating rate of 10 °C min^{-1}

Fig. S18 FT-IR spectrum of thermolyzed product at 800℃ of **2a** and **4**

Fig. S19 SEM image and EDS mapping of thermolyzed product at 800℃ of **2a**

Fig. S20 SEM image and EDS mapping of thermolyzed product at 800℃ of **4**

Fig. S21 Single pulse solid-state ^{31}P NMR spectra of **2a-800 ℃** and **4-800 ℃**

Fig. S22 Elemental analysis CHN values of compound **1**

Fig. S23 Elemental analysis CHN values of compound **2a**

Fig. S24 Elemental analysis CHN values of Compound **2b** (formed by in-situ conversion of **1** to **2b**)

Fig. S25 Elemental analysis CHN values of compound **3**

Fig. S26 Elemental analysis CHN values of compound **4**

Fig. S27 Elemental analysis CHN values of Compound **4** (formed by in-situ conversion of **3** to **4**)

Table S1. Continuous Shape measures of the coordination polyhedra of tetra-coordinated Zn(II) in **1**

Table S2. Continuous Shape measures of the coordination polyhedra of tetra-coordinated Zn(II) in **3**

Table S3. Selected bond lengths [Å] for **1** and **3**

Table S4. Selected bond angles [°] for **1** and **3**

Table S5. Interlayer spacing for various complexes of n-octyl and n-hexyl phosphate

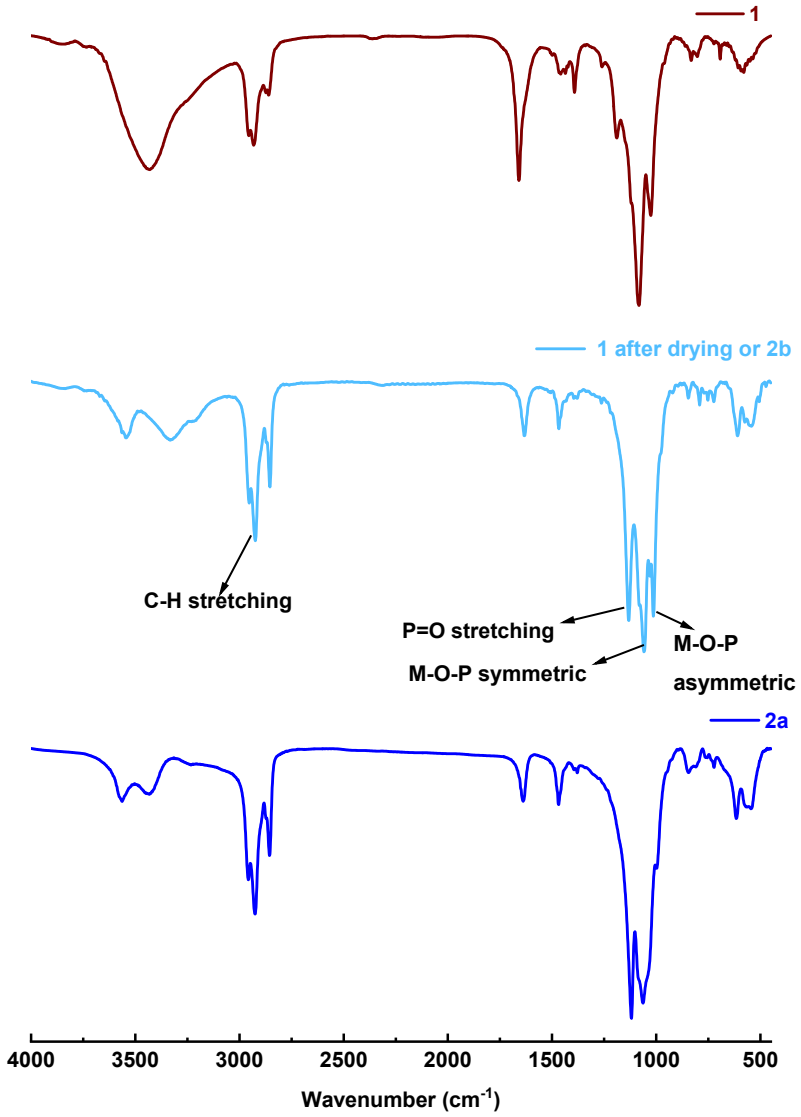

Fig. S1 FT-IR spectra of **1**, **2a,** and **2b** as KBr pellets.

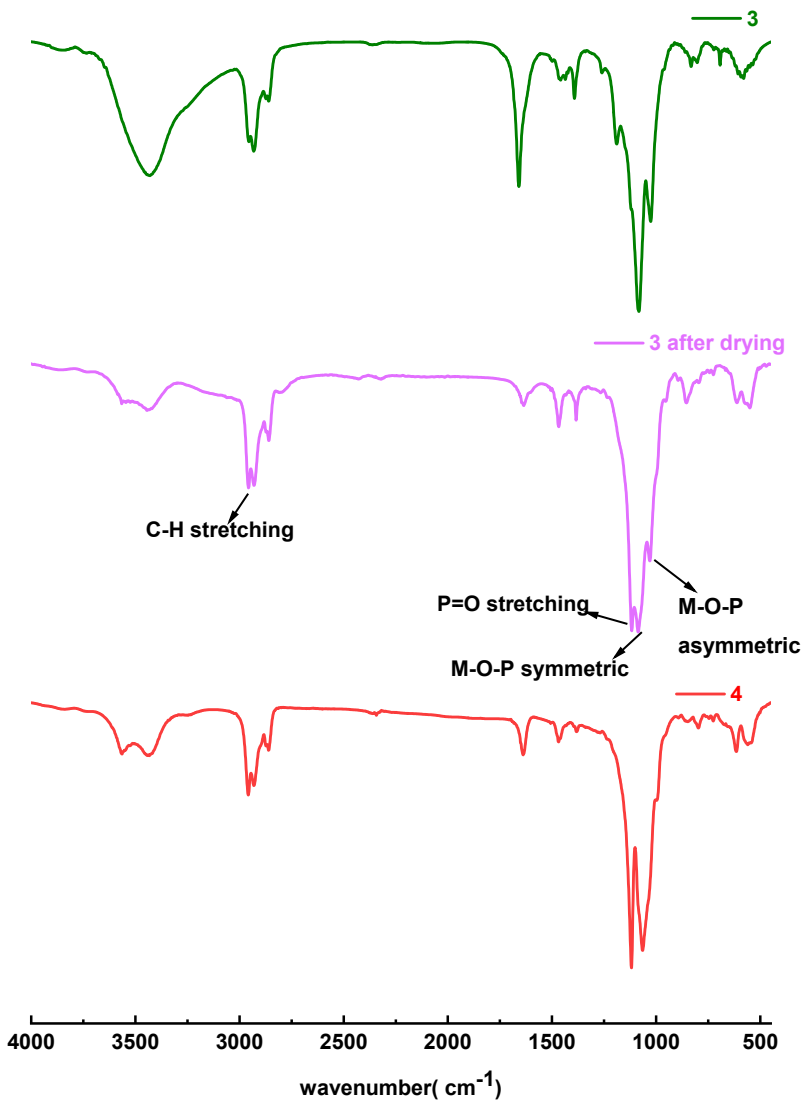

Fig. S2 FT-IR spectra of **3** and **4** as KBr pellets.

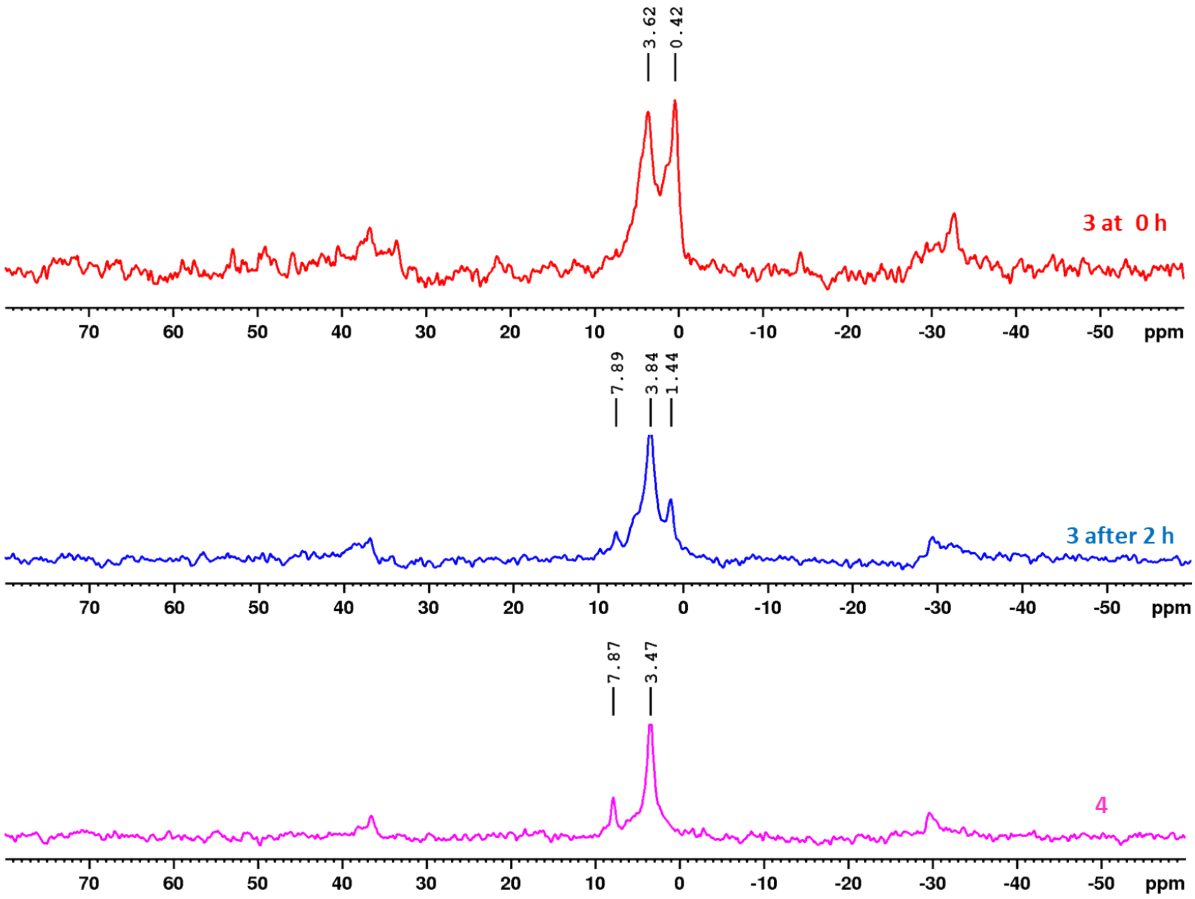

Fig. S3 ^{31}P CP-MAS NMR spectra of **3** and **4** (303 MHz).

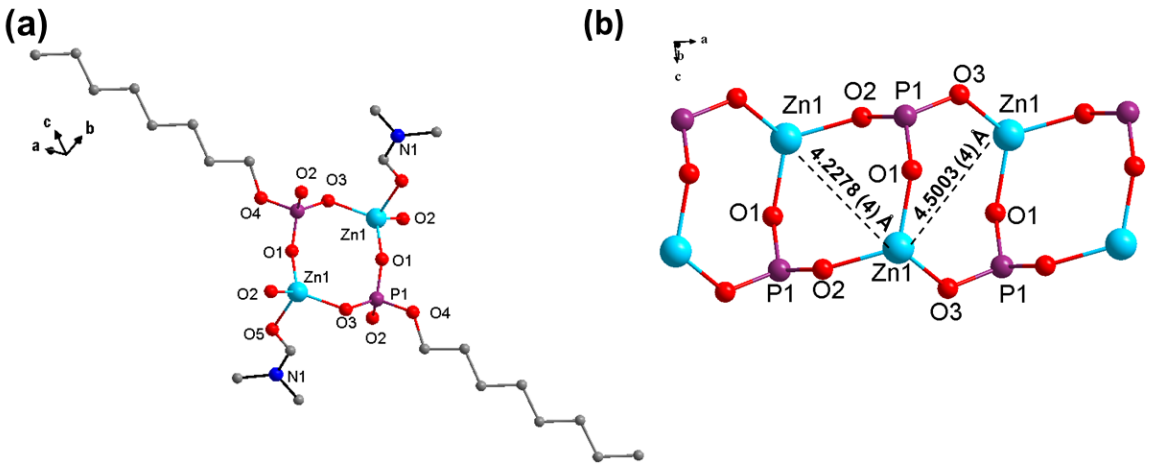

Fig. S4 Molecular structure of [^{n}OctOPO$_3$Zn(DMF)]$_n$ (**1**) (a) S4R ring in the polymeric structure (b) Edge sharing S4R rings (Hydrogen atoms are omitted for clarity; Colour Scheme; ●: Zn, ●: P, ●:O, ●: N, ●: C)

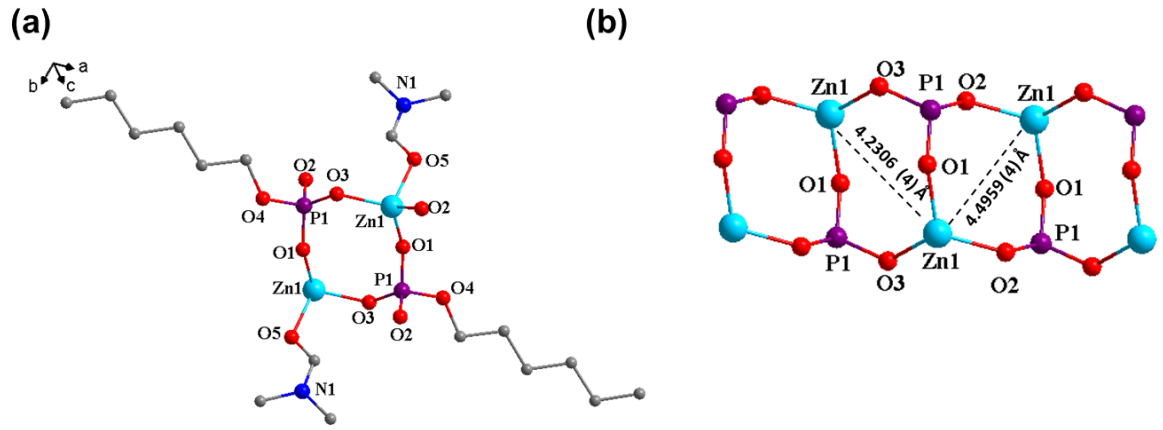

Fig.S5 Molecular structure of $[^{n}HexOPO_3Zn(DMF)]_n$ (**3**) (a) S4R ring in the polymeric structure (b) Edge sharing S4R rings (Hydrogen atoms are omitted for clarity; Colour Scheme; ●: Zn, ●: P, ●:O, ●: N, ●: C).

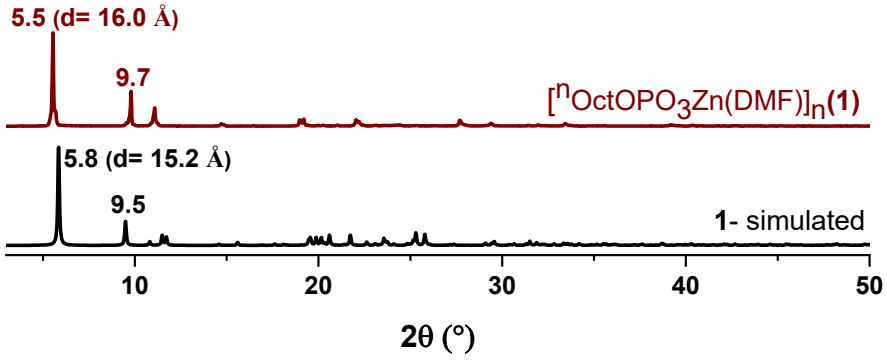

Fig. S6 Experimental and simulated Powder XRD pattern of **1**.

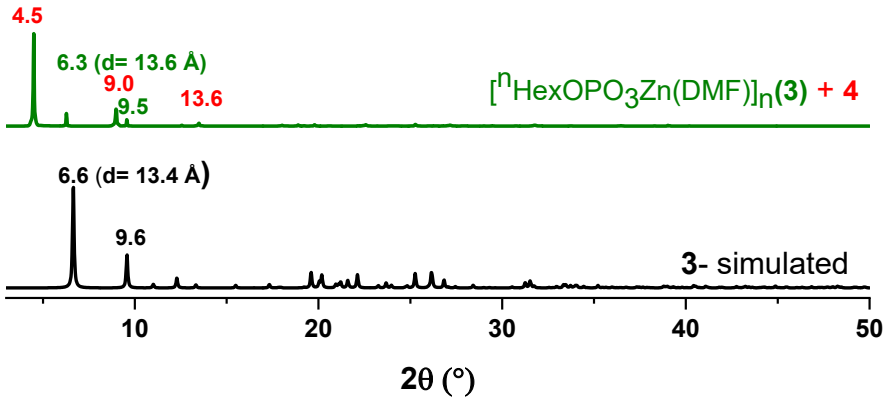

Fig. S7 Experimental and simulated powder XRD pattern of **3**; pure experimental PXRD for **3** could not be obtained due to rapid solvent exchange.

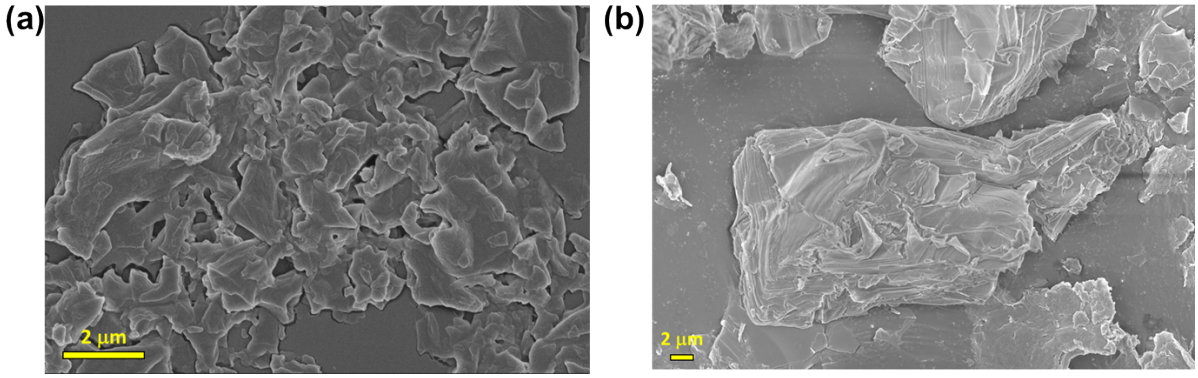

Fig. S8 SEM image of (a) **2a** and (b) **3** showing layered morphology.

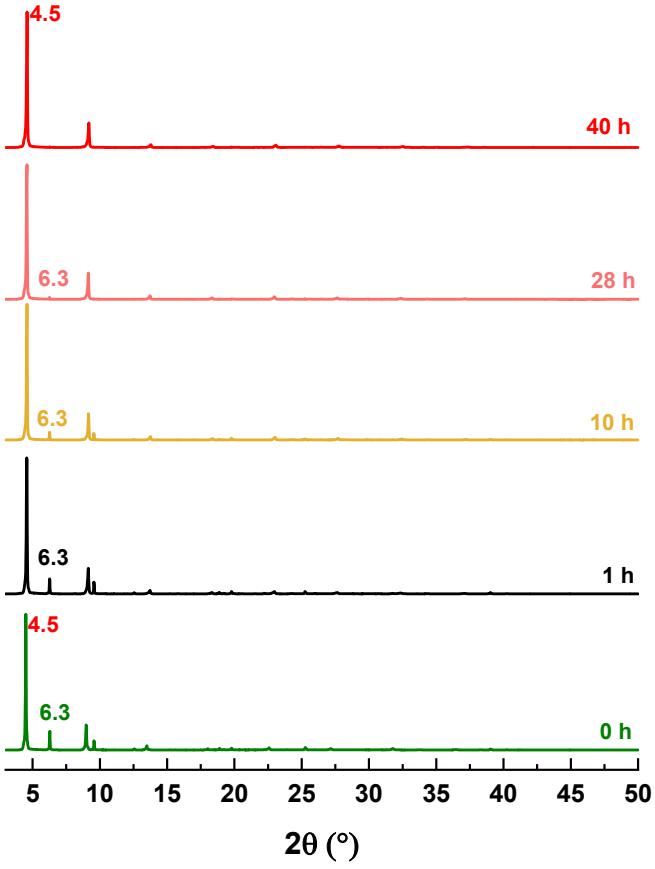

Fig. S9 Powder XRD patterns showing structure evolution of **4** from a mixture of **3** and **4**; pure experimental PXRD for **3** could not be obtained due to rapid solvent exchange (6.3º: 001 reflection for **3**; 4.5º: 001 reflection for **4**)

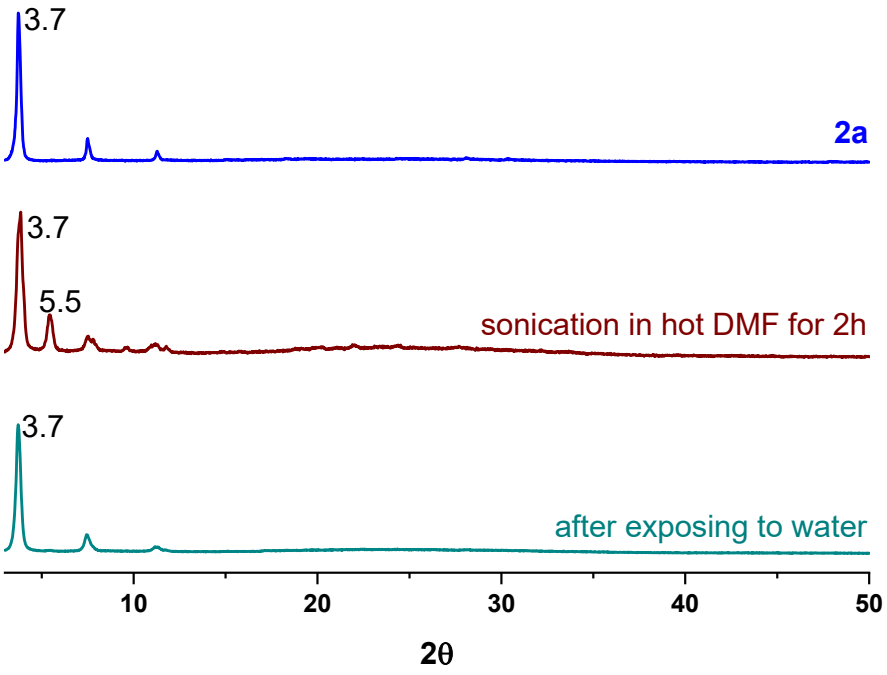

Fig S10. PXRD patterns of **2a** before and after two hours of sonication in DMF at 50 °C, followed by exposure to water, demonstrating the reversible nature of the DMF–water exchange. (5.5º: 001 reflection for **1**; 3.7º: 001 reflection for **2a**)

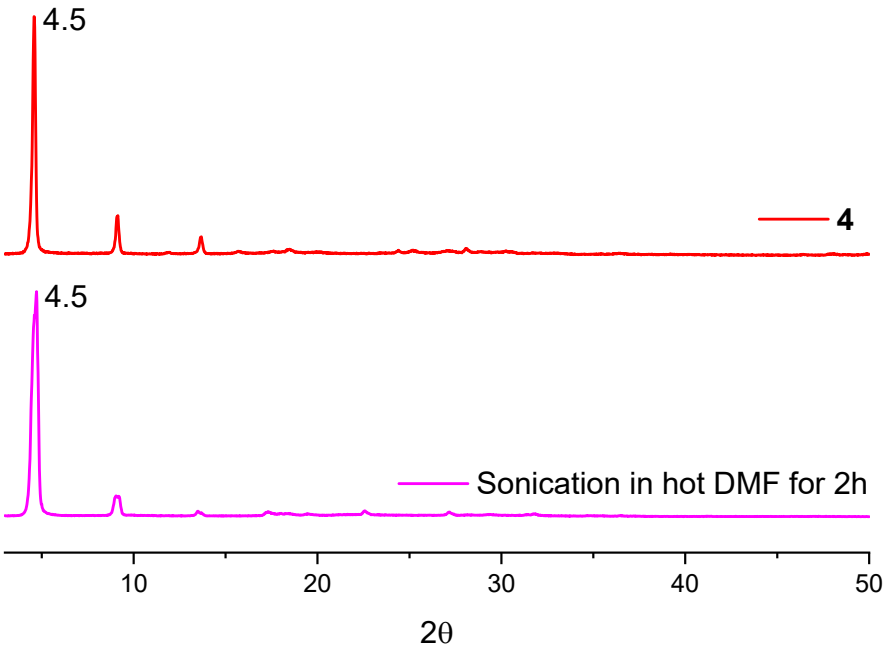

Fig S11. PXRD patterns of **4** before and after two hours of sonication in DMF at 50 °C, demonstrating the irreversible nature of the DMF–water exchange.

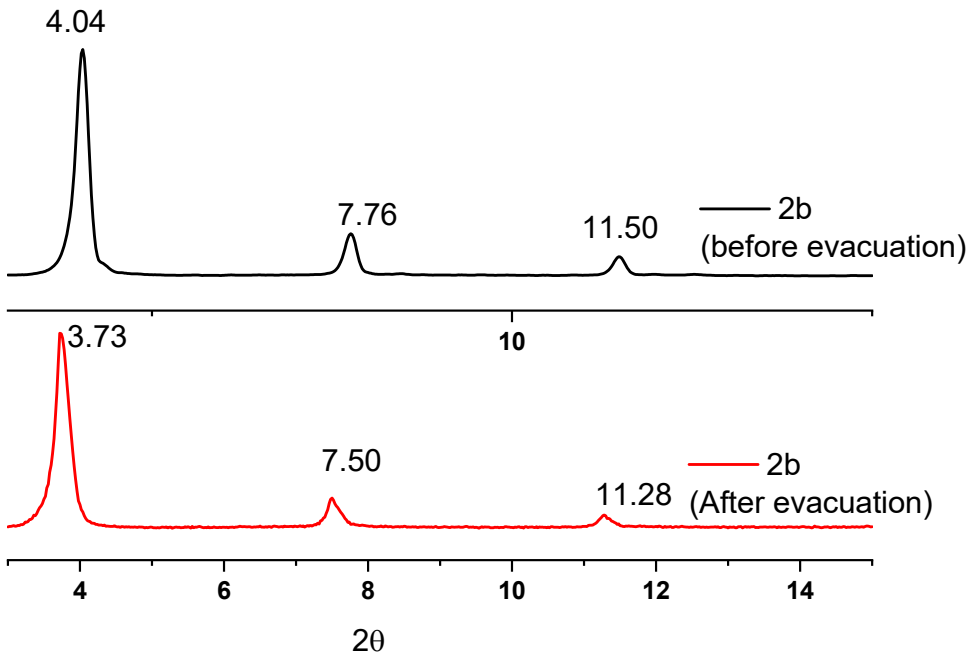

Fig S12. PXRD patterns of **2b** before and after heating at 50 °C under vacuum for 20 hours, showing its conversion back to **2a.**

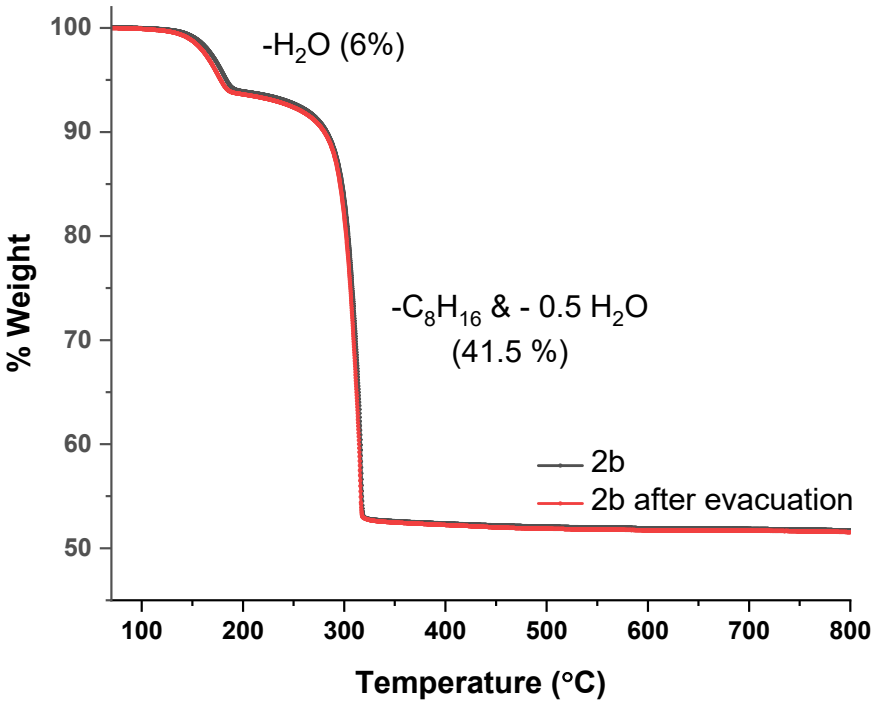

Fig S13. TGA curves of **2b** before and after heating at 50 °C under vacuum for 20 hours, indicating that **2a** and **2b** have similar chemical composition.

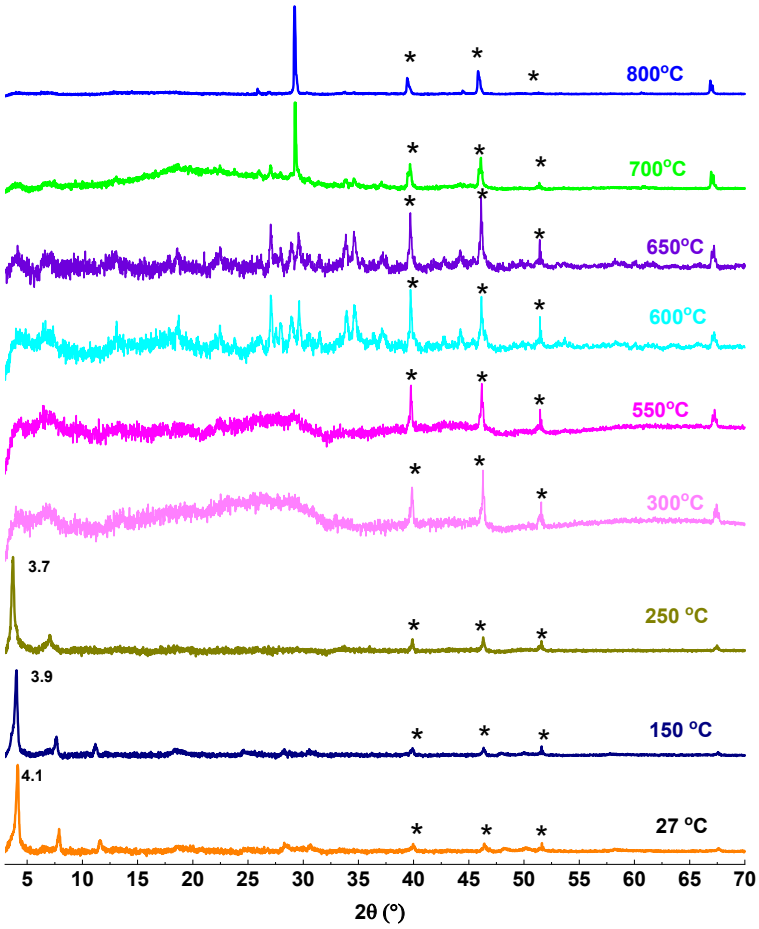

Fig. S14. Variable temperature PXRD of **2b** showing the formation of an amorphous phase at 300 °C and a crystalline phase at 800 °C (* corresponds to the peaks due to platinum sample holder).

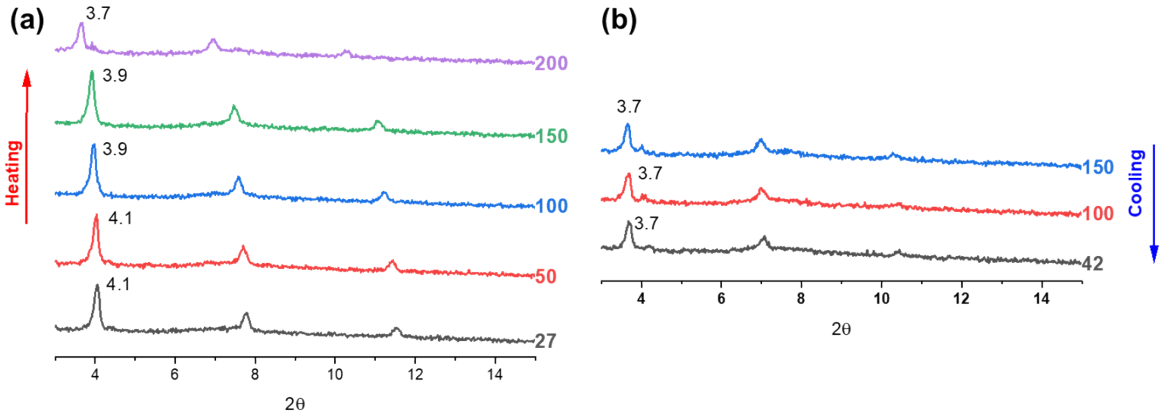

Fig. S15. Variable temperature PXRD plots of **2b** during (a) heating and (b) cooling, showing an increase in interlayer distance with increase in temperature.

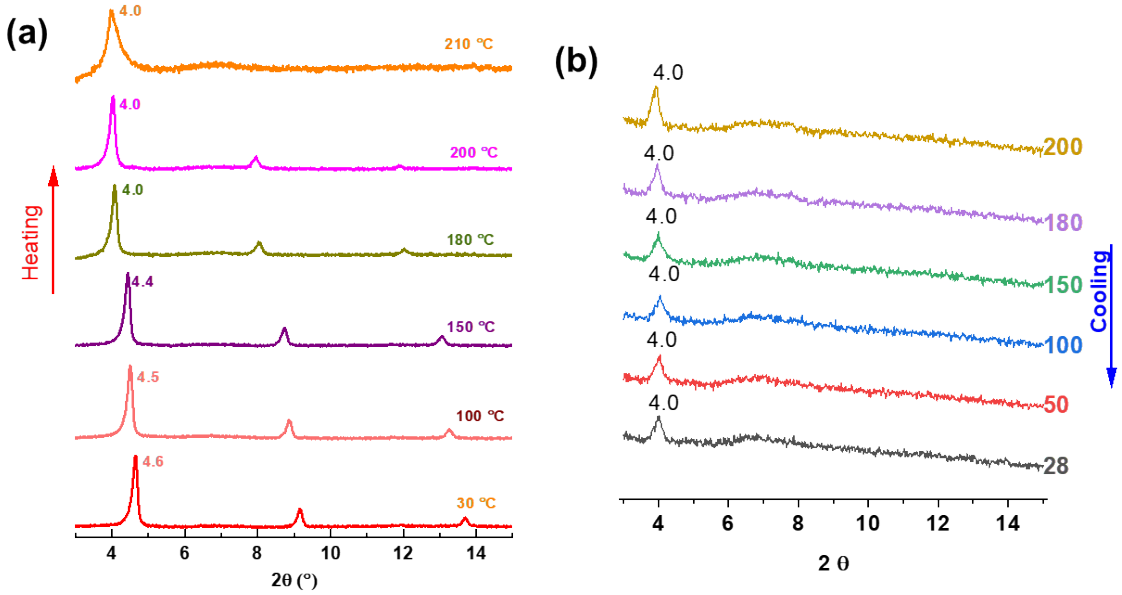

Fig. S16. Variable temperature PXRD plots of **4** during (a) heating, and (b) cooling, showing an increase in interlayer distance with increase in temperature.

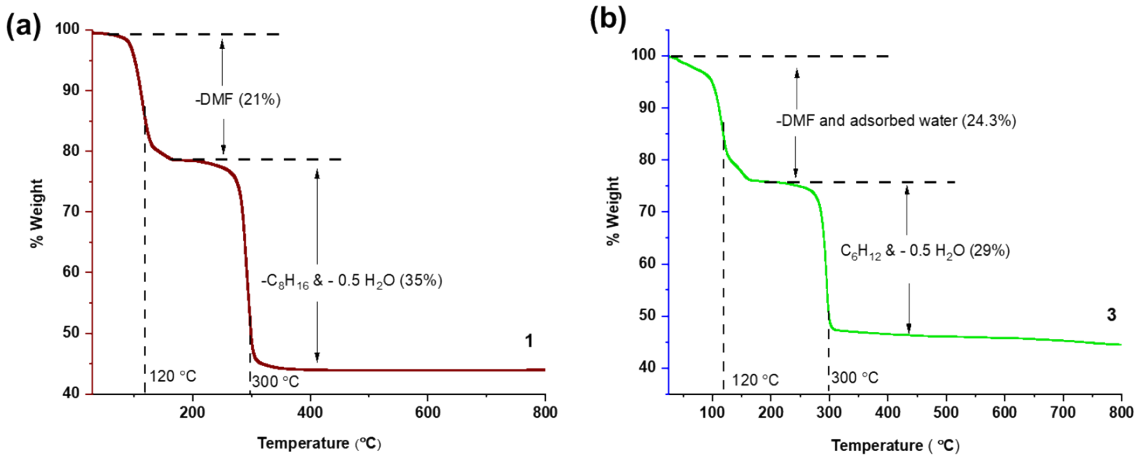

Fig. S17 TGA-DTA traces of (a) **1** and (b) **3** recorded under a flow of N_2 at a heating rate of 10 °C min^{-1}.

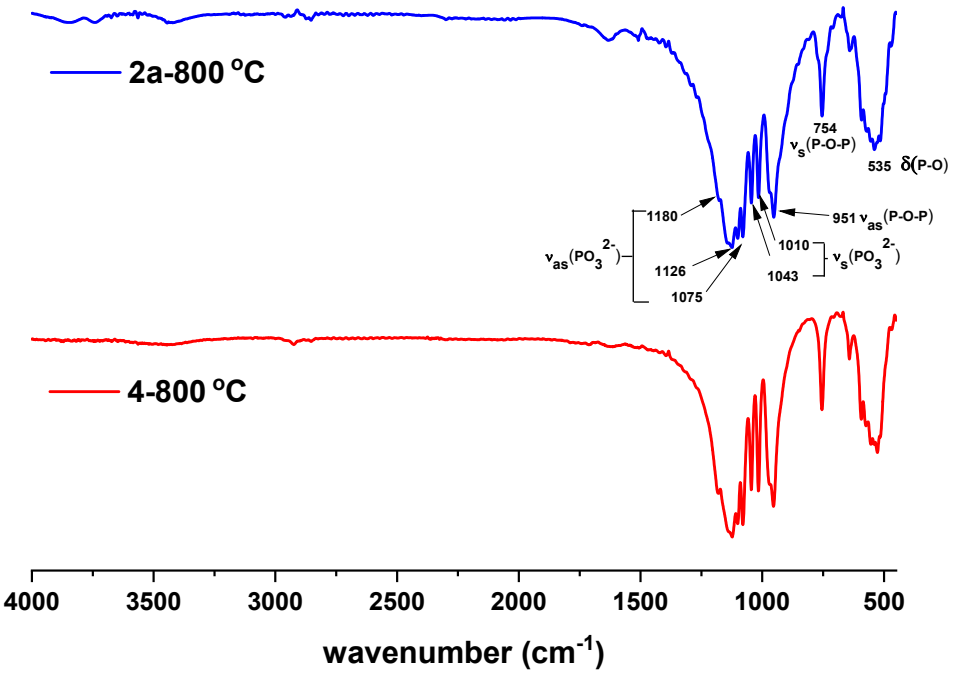

.

Fig. S18 FT-IR spectrum of thermolyzed product at 800℃ of **2a** and **4** (as KBR pellet).

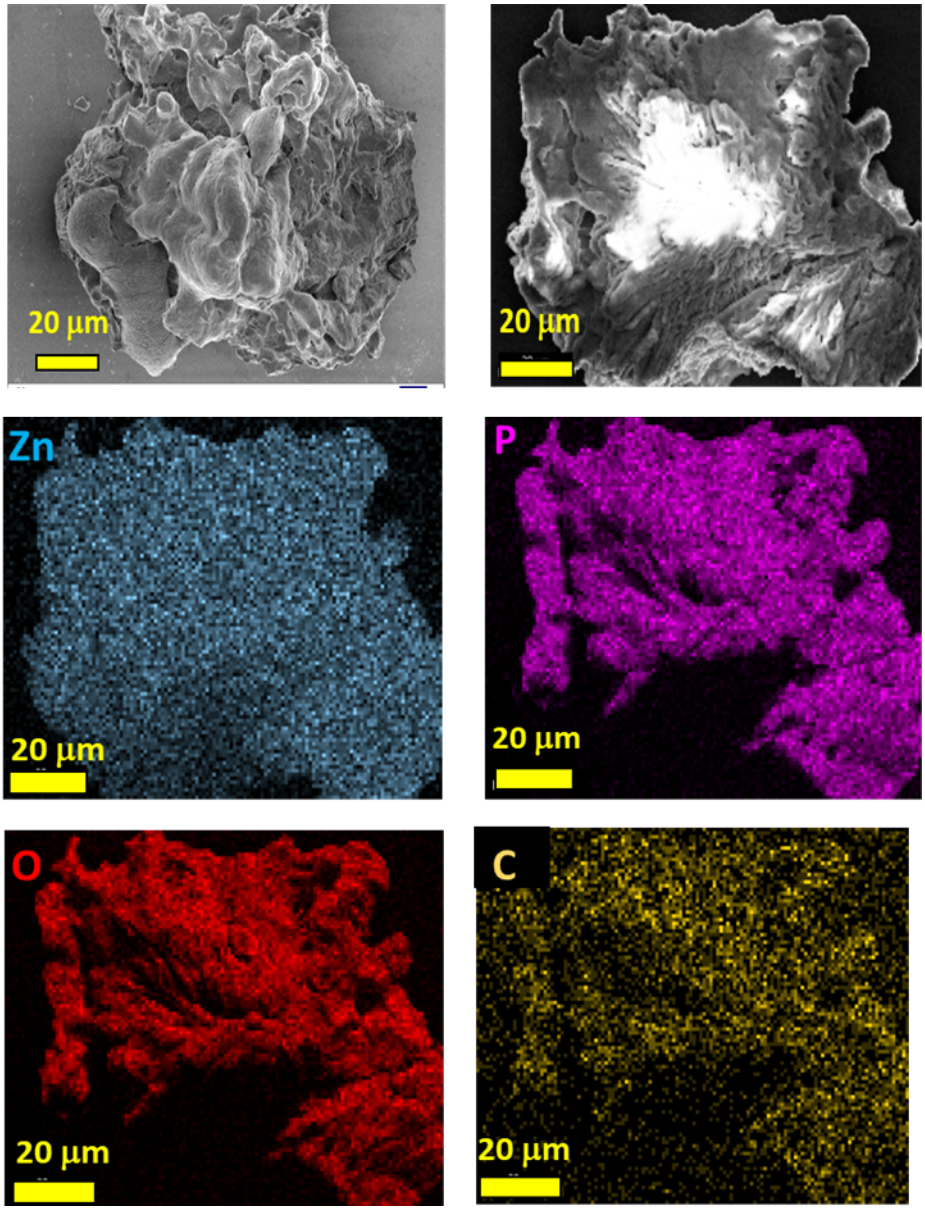

Fig. S19 SEM image and EDS mapping of thermolyzed product at 800°C of **2a**.

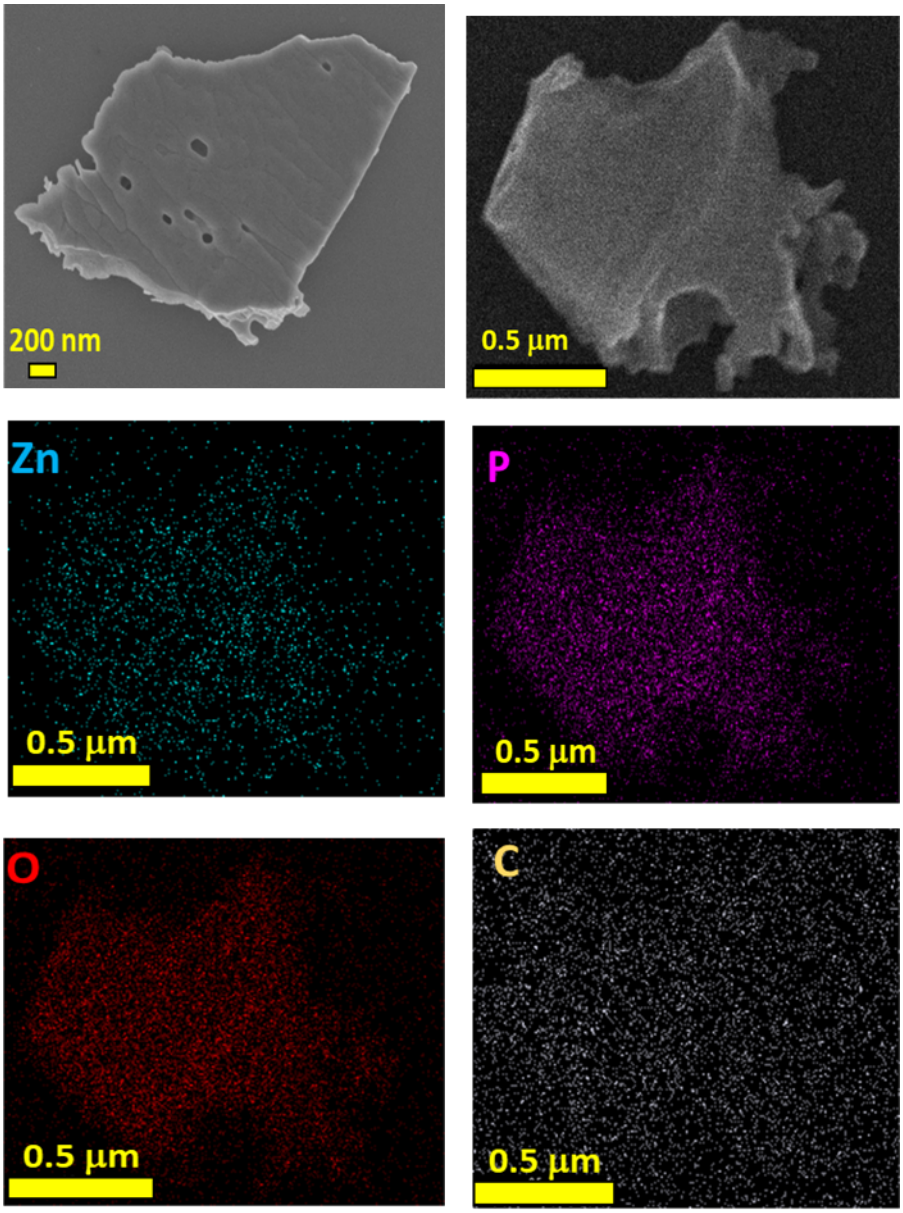

Fig. S20 SEM image and EDS mapping of thermolyzed product at 800℃ of **4**.

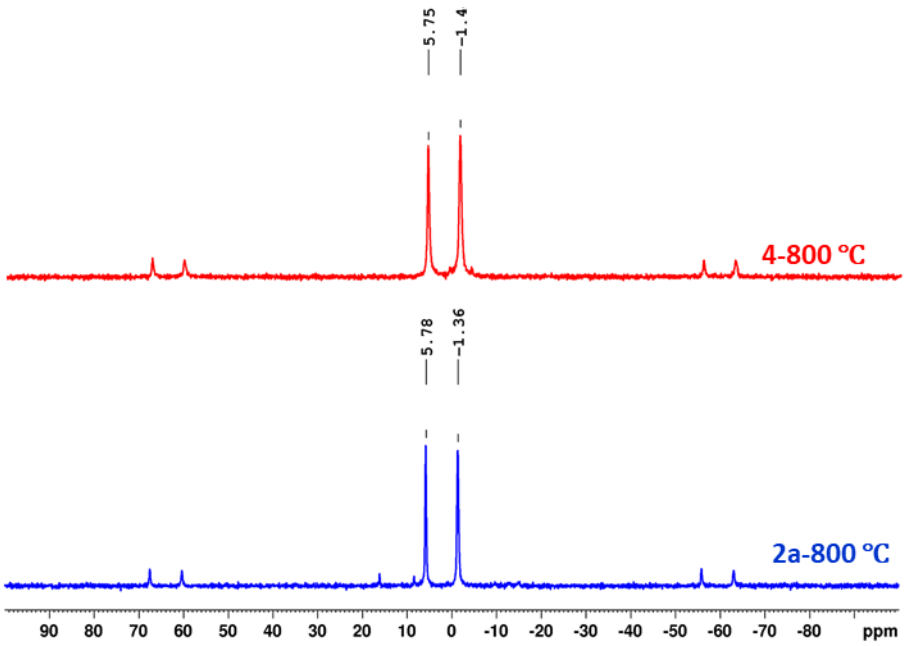

Fig. S21 Single pulse solid-state ^{31}P NMR spectra of **2a-800 °C** and **4-800 °C** (162 MHz).

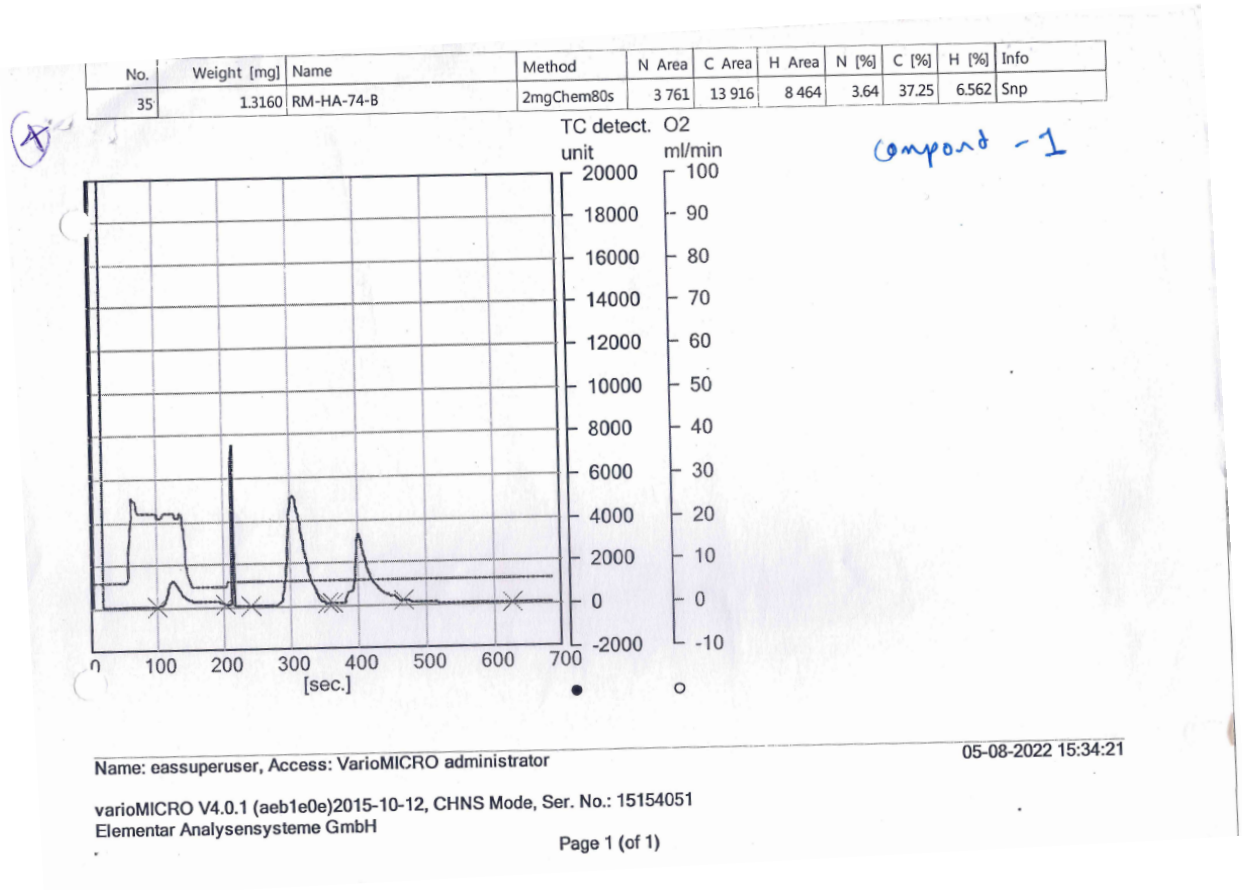

Fig. S22 Elemental analysis CHN values of compound **1**.

Document: CHNS14032024 (varioMICRO) from: 15-03-2024 09:44:16

SP18022016
varioMICRO CHNS
serial number: 15154051

Compound 2

Graphic report

No.	Weight [mg]	Name	Method	N Area	C Area	H Area	N [%]	C [%]	H [%]	Date Time
47	1.1150	RM-HA-74	2mgChem80s	1 857	10 439	6 250	0.00	32.85	6.354	14-03-2024 20:11

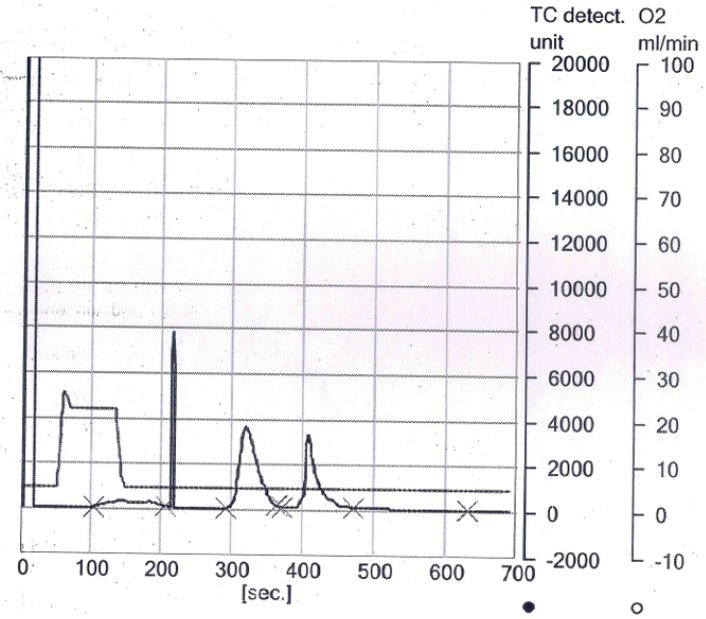

Fig. S23 Elemental analysis CHN values of compound **2a**.

No.	Weight [mg]	Name	Method	N Area	C Area	H Area	N [%]	C [%]	H [%]	Date Time
46	1.6900	RM-HA-74-CRY	2mgChem80s	1 923	16 102	9 674	0.00	33.27	6.589	14-03-2024 19:59

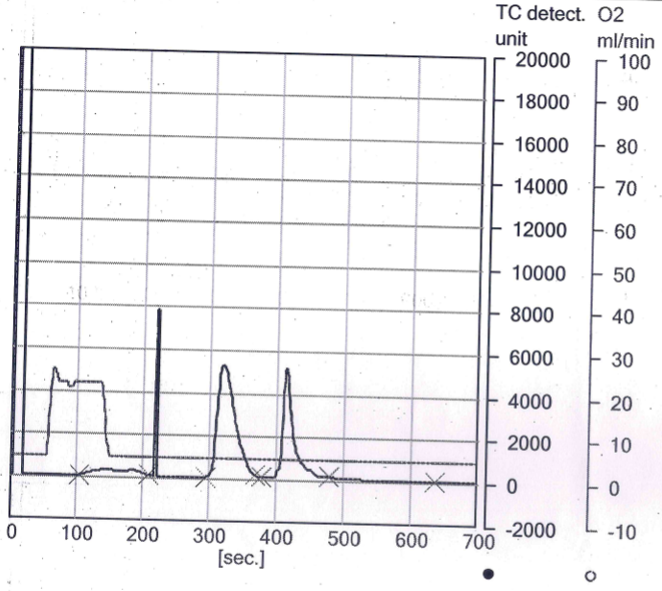

Compound 1 - after drying

Name: eassuperuser, Access: VarioMICRO administrator

18-03-2024 09:34:06

varioMICRO V4.0.1 (aeb1e0e)2015-10-12, CHNS Mode, Ser. No.: 15154051
Elementar Analysensysteme GmbH

Page 1 (of 2)

Fig. S24 Elemental analysis CHN values of Compound **2b** (formed by in-situ conversion of **1** to **2b**).

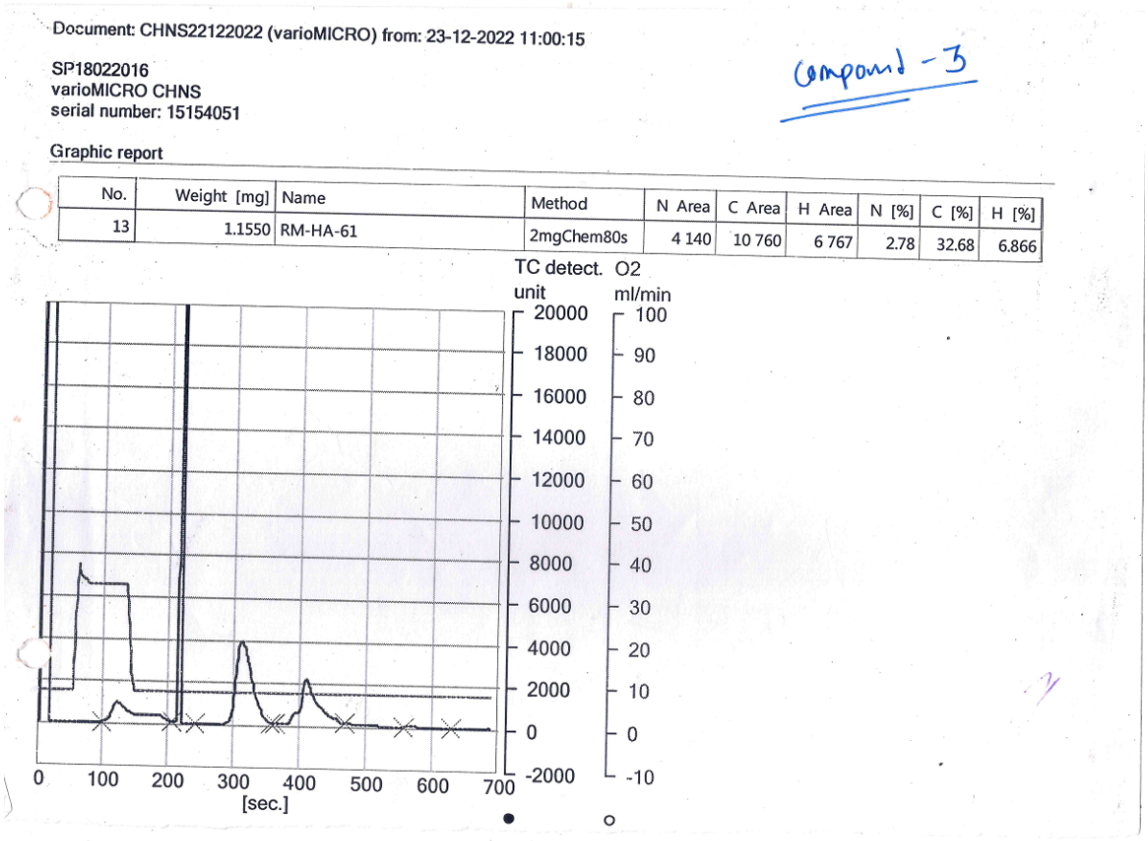

Fig. S25 Elemental analysis CHN values of compound **3**.

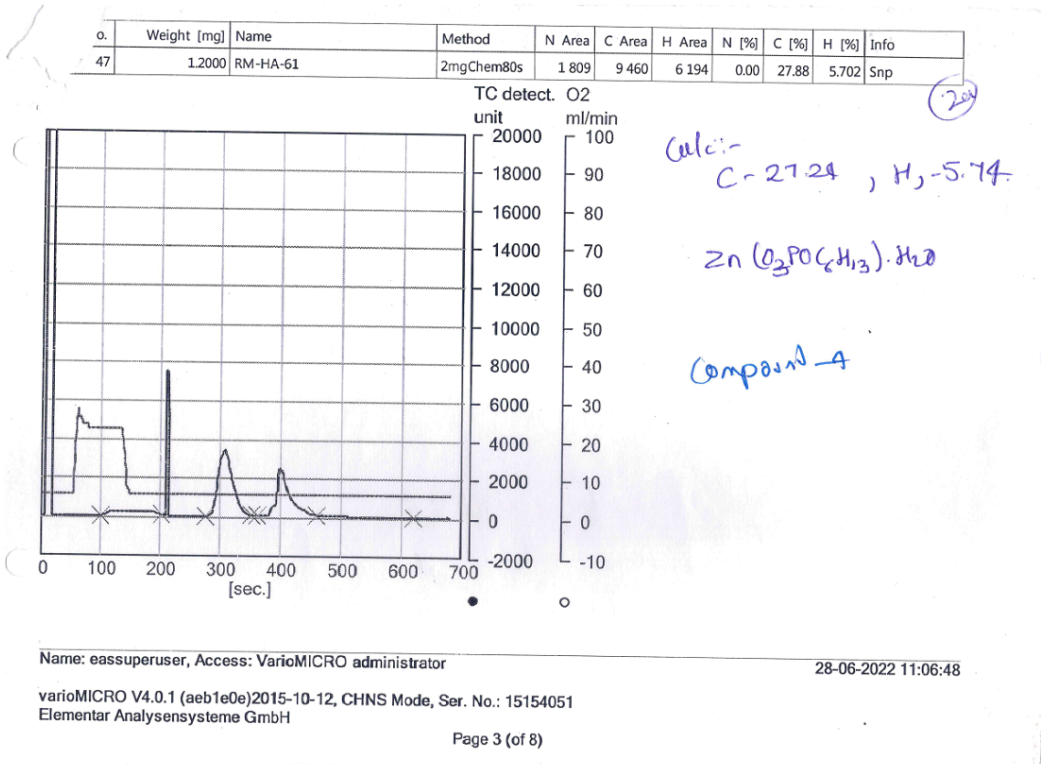

Fig. S26 Elemental analysis CHN values of compound **4**.

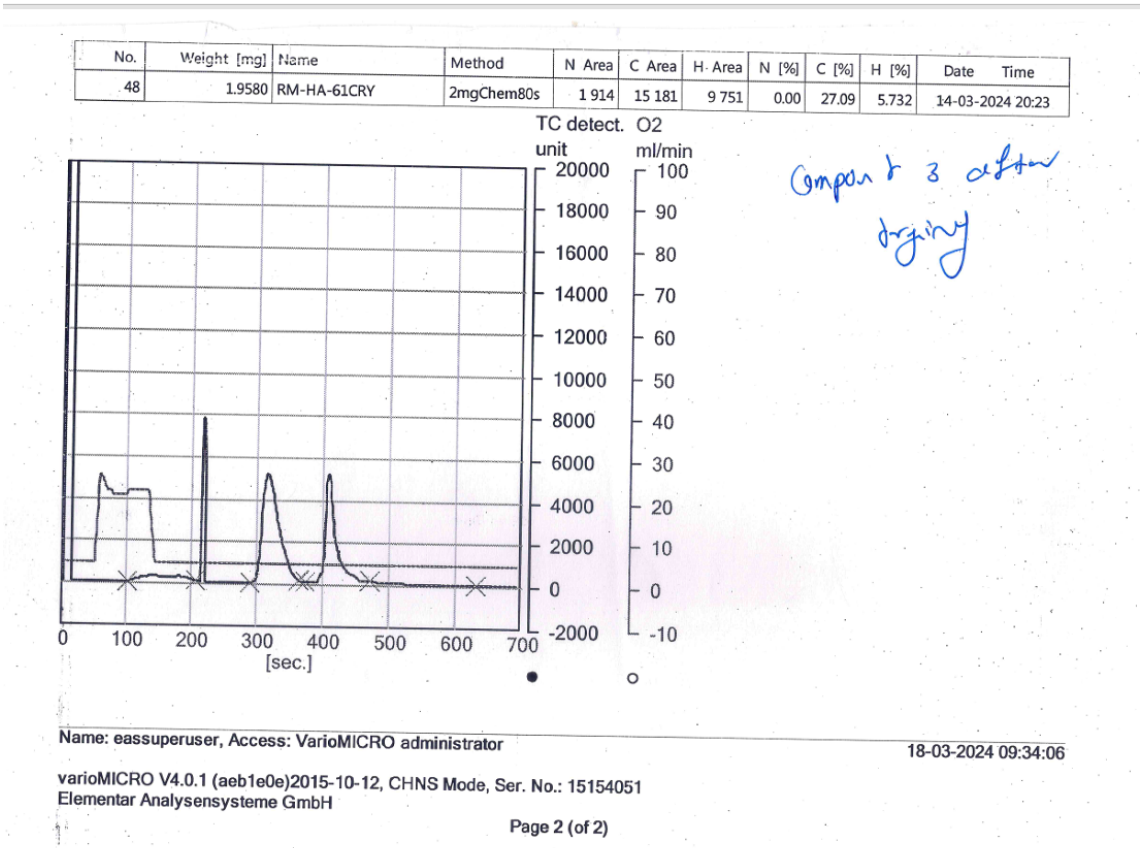

No.	Weight [mg]	Name	Method	N Area	C Area	H Area	N [%]	C [%]	H [%]	Date Time
48	1.9580	RM-HA-61CRY	2mgChem80s	1 914	15 181	9 751	0.00	27.09	5.732	14-03-2024 20:23

Fig. S27 Elemental analysis CHN values of Compound **4** (formed by in-situ conversion of **3** to **4**).

Table S1. Continuous Shape measures of the coordination polyhedra of tetra-coordinated Zn(II) in **1**.

Label	**Symmetry**	**Shape**	**Deviation**
SP-4	D4h	Square	32.744
T-4	Td	Tetrahedron	0.354
SS-4	C2v	Seesaw	8.503
vTBPY-4	C3v	Vacant trigonal bipyramid	1.841

Table S2. Continuous Shape measures of the coordination polyhedra of tetra-coordinated Zn(II) in **3**.

Label	**Symmetry**	**Shape**	**Deviation**
SP-4	D4h	Square	32.612
T-4	Td	Tetrahedron	0.359
SS-4	C2v	Seesaw	8.463
vTBPY-4	C3v	Vacant trigonal bipyramid	1.843

Table S3. Selected bond lengths [Å] for **1** and **3**.

1	
Zn1-O3[1]	1.925(2)
Zn1-O5	2.025(2)
Zn1-O2	1.910(2)
Zn1-O1[2]	1.914(2)
P1-O3	1.521(2)
P1-O2	1.522(2)
P1-O4	1.594(2)
P1-O1	1.505(2)
O5-C9	1.256(3)
O4-C1	1.439(3)
N1-C9	1.313(3)
N1-C11	1.458(3)
N1-C10	1.464(3)
C2-C1	1.508(3)
C2-C3	1.519(3)
C3-C4	1.527(3)
C4-C5	1.527(3)
C6-C5	1.526(3)
C6-C7	1.522(3)
C8-C7	1.515(4)

[1]-1+X,+Y,+Z; [2]1-X,1-Y,2-Z

3	
Zn1-O3[1]	1.928(1)
Zn1-O5	2.023(2)
Zn1-O2	1.912(1)
Zn1-O1[2]	1.913(1)
P1-O3	1.521(1)
P1-O2	1.526(1)
P1-O4	1.595(1)
P1-O1	1.510(1)
O5-C7	1.258(2)
O4-C1	1.442(2)
N1-C7	1.313(3)
N1-C8	1.466(3)
N1-C9	1.462(3)
C1-C2	1.510(3)
C3-C2	1.523(3)
C3-C4	1.526(3)
C4-C5	1.521(3)
C5-C6	1.523(3)

[1]-1+X,+Y,+Z; [2]1-X,1-Y,2-Z

Table S4. Selected bond angles [°] for **1** and **3**.

1	
O3[1]-Zn1-O5	104.11(6)
O2-Zn1-O3[1]	115.53(7)
O2-Zn1-O5	103.97(6)
O2-Zn1-O1[2]	115.69(7)
O1[2]-Zn1-O3[1]	114.69(7)
O1[2]-Zn1-O5	100.00(7)
O3-P1-O2	109.75(9)
O3-P1-O4	107.66(9)
O2-P1-O4	108.98(9)
O1-P1-O3	112.86(9)
O1-P1-O2	114.65(9)
O1-P1-O4	102.42(9)
P1-O3-Zn1[3]	125.34(9)
C9-O5-Zn1	119.9(1)
P1-O2-Zn1	134.7(1)
C1-O4-P1	122.5(1)
P1-O1-Zn1[2]	144.5(1)
C9-N1-C11	122.6(2)
C9-N1-C10	120.6(2)
C11-N1-C10	116.7(2)
O5-C9-N1	123.7(2)
C1-C2-C3	113.6(2)
O4-C1-C2	107.1(2)
C2-C3-C4	112.3(2)
C3-C4-C5	113.4(2)
C6-C5-C4	113.2(2)
C8-C7-C6	113.5(2)
C7-C6-C5	113.4(2)

[1]-1+X,+Y,+Z; [2]1-X,1-Y,2-Z; [3]1+X,+Y,+Z

3	
O3[1]-Zn1-O5	104.31(6)
O2-Zn1-O3[1]	114.90(6)
O2-Zn1-O5	103.88(6)
O2-Zn1-O1[2]	115.83(6)
O1[2]-Zn1-O3[1]	115.19(6)
O1[2]-Zn1-O5	99.92(6)
O3-P1-O2	109.75(8)
O3-P1-O4	107.80(8)
O2-P1-O4	108.76(8)
O1-P1-O3	112.94(8)
O1-P1-O2	114.68(8)
O1-P1-O4	102.39(8)
P1-O3-Zn1[3]	125.09(8)
C7-O5-Zn1	120.0(1)
P1-O2-Zn1	133.89(9)
C1-O4-P1	122.4(1)
P1-O1-Zn1[2]	145.54(9)
C7-N1-C8	122.2(2)
C7-N1-C9	120.8(2)
C9-N1-C8	116.9(2)
O5-C7-N1	124.1(2)
C1-C2-C3	113.9(2)
O4-C1-C2	107.0(2)
C2-C3-C4	112.5(2)
C5-C4-C3	113.9(2)
C4-C5-C6	113.2(2)

[1]-1+X,+Y,+Z; [2]1-X,1-Y,2-Z; [3]1+X,+Y,+Z

Table S5. Interlayer spacing for various complexes of n-octyl and n-hexyl phosphate.

Sr. No.	Metal	Interlayer spacing (Å)		Ref.
		Octyl	Hexyl	
1	Mg	24.7	20.7	[1]
2	Ca	23.9	18.0, 20.1	[2, 3]
3	Sr	23.6	20.6	[3]
4	Ti	24.4	20.4	[4]
5	Fe	26.0	-	[5]
6	Zr	23.0	21.0	[6]
7	Al	27.0, 21.0	22.0, 18.0	[7, 8]
8	Zn	23.8, 21.6	19.6	This work

References:

1. M. Cave, D. Farrar and A. J. Wright, *Key Eng. Mater.*, 2008, **361**, 383-386.
2. H. Tanaka, T. Watanabe, M. Chikazawa, K. Kandori and T. Ishikawa, *Colloids Surf. A: Physicochem. Eng. Asp.*, 1998, **139**, 341-349.
3. M. R. Cave, Investigation of layered calcium phosphates and related materials for Biomaterial applications, *Ph.D. Thesis*, University of Birmingham, 2010.
4. H. Tanaka, K. Masuda and R. Hino, *J. Colloid Interface Sci.*, 2002, **254**, 331-337.
5. H. Tanaka, K. Taniguchi and R. Hino, *Phosphorus Res. Bull.*, 2005, **19**, 268-273.
6. S. Yamanaka, M. Matsunaga and M. Hattori, *J. Inorg. Nucl. Chem.*, 1981, **43**, 1343-1346.
7. H. Tanaka and M. Chikazawa, *J. Mater. Chem.*, 1999, **9**, 2923-2927.
8. H. Tanaka and M. Chikazawa, *Mater. Res. Bull.*, 2000, **35**, 75-84.